NURETH14-131

EXPERIMENTAL INVESTIGATION AND MODELLING OF BULK BOILING FOR CFD APPLICATION

J. Kutnjak, R. Kulenovic and E. Laurien

University of Stuttgart, Institute for Nuclear Technology and Energy Systems, Stuttgart, Germany

josip.kutnjak@ike.uni-stuttgart.de, rudi.kulenovic@ike.uni-stuttgart.de, eckart.laurien@ike.uni-stuttgart.de

Abstract

Bulk boiling is a phenomenon characterised by production of vapour inside a liquid away from heating surfaces. This boiling phenomenon is of interest in reactor safety considerations about de-pressurisation of heated pressurised reactor systems. For observation of such flow phenomena a test set-up is available working with de-mineralised water at ambient pressure. The bubble behaviour is visualised within an observation volume and is recorded using a video camera. Vapour formation and bubble behaviour are evaluated using digital video processing. The experimental data are used for comparison with transient computational fluid dynamics simulations.

1. Introduction

1.1 Motivation

Among nuclear accident scenarios there are several cases that involve bulk boiling phenomena, e.g. pressure loss in the primary circuit. As the water in the pressurised circuit becomes superheated due to the reduction of pressure, wall boiling models for heated surfaces cannot be applied. Additionally bulk boiling often involves two-phase instabilities such as flashing and geysering that might damage parts of the facility. Therefore, the fundamental mechanisms and their understanding are of great interest in reactor safety as well as in other disciplines.

To observe such phenomena and derive mechanisms from that experience an experimental setup has been built at IKE. The observation and measurements are used as base for modelling of the process. Current Computational Fluid Dynamics (CFD) doesn't offer an advanced model that is suited for calculation of steam production during boiling in the bulk of the liquid. However, the 'two-fluid model' [11] used in current CFD can calculate non-equilibrium thermodynamics in the source/sink term of the transport equations that determines the mass transfer between the phases liquid and vapour. Several forces are acting between the phases involving buoyancy force, drag force and others, and they strongly influence turbulence and mixing and therefore the previously mentioned heat transfer between the phases. To determine all these quantities the usually unknown bubble diameter still needs to be specified by the user. However a prescribed constant bubble diameter affects all forces, turbulence, mixing and the interfacial area needed for the

heat/mass transfer. Therefore, modelling of the bubble diameter is a mandatory goal for improved calculation quality.

1.2 Literature status

Bubble creation inside a liquid volume, droplets emerging from steam, crystals growing from liquids and numerous other physical phenomena encountered in nature and technology are yet to be understood. The process of the creation of clusters during a phase change is usually referred to as nucleation. The physical definition for a nucleus was first given by Volmer and Weber [1]. Later, based on that definition, the classical theory for nucleation was introduced by Becker and Döring who gave an expression that can calculate nucleation rates [2].

Experimental investigations directly measuring nucleation rates were conducted by several authors for various substances. Miller et al. used an expansion cloud chamber to investigate homogeneous nucleation rates for water over a wide range of temperature and nucleation rates from 10^6 - 10^{12} drops m⁻³ s⁻¹ [3].

Later Viisanen et al. used the nucleation pulse technique to measure nucleation rates from 10¹¹ to 10¹⁵ m⁻³ s⁻¹ [4]. The data analysis had qualitative agreement in the range of overlap with Millers results. Comparison to classical theory showed at some points exact agreement, and partly higher partly lower temperature dependency in the theory. They concluded that there is serious disagreement between their measurements and the theory.

Wölk and Strey summarized several authors measurements of nucleation rates in light and heavy water ranging from $1x10^6$ to $6x10^{21}$ m⁻³ s⁻¹ [5]. Based on these collected measurements they introduced an empirically corrected function for homogeneous nucleation rates in water correcting the Becker/Döring theory with an additional factor.

Various other experimental investigations with more macroscopical background were conducted. Many involve non-invasive optical measurements including object recognition and tracking methods. Rong investigated subcooled boiling in a vertical annular channel with an inserted heater rod using high speed video recordings [6]. The focus was on bubble departure frequencies and lift-off diameters, as well as bubble growth rates and velocities after lift-off. Another study has been conducted by Zaruba that used a rectangular water column of 1.5 m height [7]. At the center of the bottom of that column air was injected and the bubbles were observed using a high speed camera. The work shows recorded bubbles being identified by using the proper digital image processing and tracking. The velocity distributions of the dispersed phase were measured and the turbulent diffusion coefficients of the gaseous phase were calculated using the experimental results.

A study concerning the frequency of flashing phenomena was conducted at Forschungszentrum Karlsruhe with a 6 m high water column being heated from the bottom [8]. The setup was used with and without forced convection with different heating inputs and water levels. It was stated that there was a flashing frequency found, but below a water level of 2.5 m the mode changes to a different pattern.

Giese measured in his work how thermal cavitation increases the pressure loss through a pipe with gravity driven flow [9]. The work included CFD simulations using the Euler-Euler model to calculate the pressure loss through a pipe bend with cavitation. It was concluded that the obligatory prescription of the bubble diameter determinates the calculated pressure loss.

Investigating the matter further E. Laurien calculated pipe bends with constant bubble diameter and constant number density [10] and concluded that CFD can calculate pressure drops but again prescription of bubble size or number density determinates the pressure loss. However, it is stated the using a number density seems more physical as bubble size change are possible from initially small nuclei.

1.3 Aim of this study

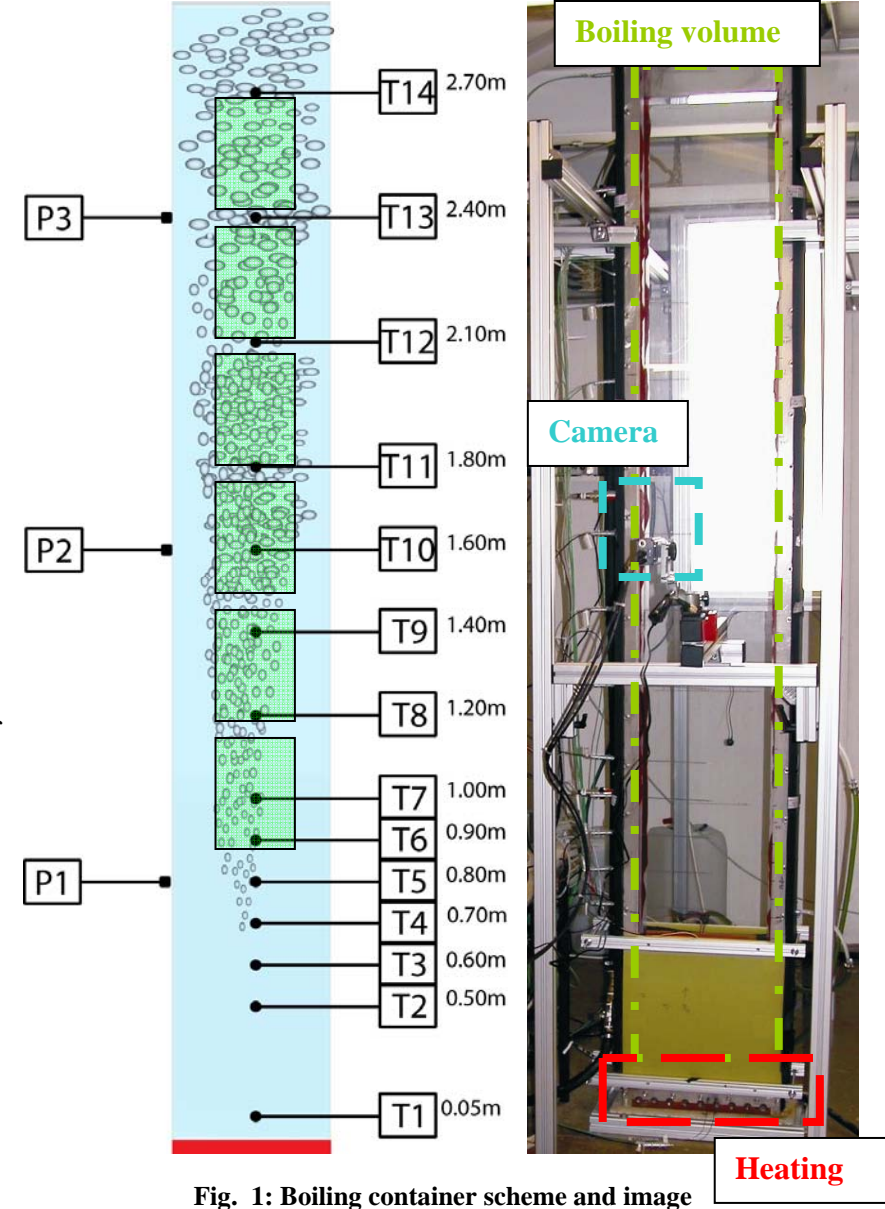
This study aims for a basic contribution in the field of thermal fluid dynamics by development of a model for transient description of bubble number densities feasible for CFD methods. In order to establish a data base for the understanding of heterogeneous bubble generation and growth processes and for model development experiments are performed in the experimental setup

described below. The results from experiments are incorporated into an algebraic model that is used in CFD simulations that reproduce the observed bubble behaviour like the growth-/shrink-effect, multiplication and possibly instabilities.

2. Experimental setup

2.1 Boiling container

The test container (Fig. consists of a 2.75 m high column of water with a rectangular horizontal cross section of 0.38 m x 0.097 m. Its main frame is made of stainless steel which holds two panes of borosilicate glass as the front and back walls. The edges of the glass plates are surrounded by a silicone-profile, which acts as a seal and avoids direct contact between the glass and metal components. materials are chemically resistant to avoid changing experimental conditions. The bottom of the container is



closed by a copper block, in which heating cartridges are installed. Altogether 9 cartridges each with a maximum electrical power of 1110 W are used, which results in a maximum heat flux of 270 kW/m². The copper surface has been polished to minimise nucleate boiling. A 19 mm layer of a closed-cell elastomer is glued to the side parts as a thermal insulation. For reduction of heat losses and to limit the heating surfaces temperature additional heating is applied via silicone heating foils directly attached to the outer side of the glass in the lower section of the container. To reduce water losses during operation above the container a heat exchanger is used to recondense the generated vapour, hence recirculate the water. The temperatures at the inlet and the outlet of the heat exchanger, as well as the mass flow are measured. The experiment runs in a quasi-steady state with constant heating temperatures of 118-120 °C at the copper blocks surface. The additional heating foils are set to 123 °C. The thermal quasi-steady state is defined as having reached an average temperature with a standard deviation below 0.5 K and maximum deviations in the range of 3 K.

Instrumentation

In the test setup temperatures are measured at several positions in the bulk volume. Shielded thermo-sensors are inserted from the sides of the container. Calibration of the measurement chain of the temperature sensors was performed with a metal-block calibrator system using the reference thermometer (Pt 1000) with a systematic uncertainty of 0.011 K. However, the data acquisition system has a resolution of 0.1 K, which is considered to be the achievable accuracy. The used temperature sensors are 9 four-wire resistance temperature detectors and 5 thermocouples of type K. Pressures are measured using absolute pressure transducers with floating piezoresistive elements at 3 different container height positions. Additionally a fourth sensor of the same type is installed in the test container's chimney. An integrated microprocessor compensates temperature changes and non-linearities, resulting in 0.1% of the total pressure range and absolute error of 30 Pa. The measured value is directly sent via an RS485 interface so that no additional error from analogue measurement needs to be accounted for.

For bubble observation the boiling process is recorded by a video camera. The camera (AVT Stingray F-125b) has a maximum resolution of 1292 x 964 Pixel @ 30 frames per second (fps), but is used with 1292 x 928 pixels at 32 fps. Using this camera the overall process is recorded continuously within a image section of 0.28 x 0.2 m². This image section was used in six positions as shown in Fig. 1 by the green areas and in Tab. 1.

Tab. 1: Vertical top end position of the image sections used

		Pos.1	Pos. 2	Pos. 3	Pos. 4	Pos.5	Pos.6
Vertical position	[m]	1.1	1.4	1.7	2.0	2.3	2.6

Lighting is provided by a white LED backlight, which generates a luminous flux of 5400 lumens on an area of 1.2x0.45 m² resolving to a lighting intensity of 10000 lux. This high light intensity offers short shutter times which avoids in-motion unsharpness.

3. Experimental results

The temperature distribution in the container generates an unstable stratification which causes single- and two-phase natural convection. Large rising plumes of high-temperature low-density liquid are observed which form streaks rising into the lower pressure regions above, where bubbles grow and slight eruptions occur. These eruptions are associated with significant vapour production. To prevent damage to the glass plates a hatch is installed in the chimney to act as a relief pressure valve. During such eruptions many bubbles are created which grow rapidly so that problems with their detection and especially their separation, arise. The eruptions can become more violent if the heat input is increased.

3.1 Pressure & temperature measurements

In Fig. 2 a typical measurement results of corresponding pressure and temperature are shown. Every pressure peak corresponds to a sharp temperature drop shortly after. On a longer time scale then the temperature of the whole container declines. The temperature measurements provide data concerning the thermal layering inside the observed volume. Due to the relatively high reaction time of the measuring elements and slow sampling rate heat peaks of rising plumes cannot be captured. However due to temperature drops during flashing the superheating can be

approximated as the water is cooled down to saturation temperature. Therefore, the amount of superheat that precedes a sudden rise in vapour fraction and bubble number can be estimated.

The pressure measurements are vital for detection of the eruptions taking place inside the container. Depending on the power of the evaporation a pressure rise can be identified inside the pressure signal. Due to the pressure relief flap the pressure rises are limited, but the rise in water level can be detected. A long time measurement of this signal was analysed using a Fast-Fourier-Transformation to check for any regular frequency behaviour but the signal didn't contain any distinct frequency. On the other hand counting of the peaks over a period of time shows that the number of eruptions per hour is nearly constant but erratic.

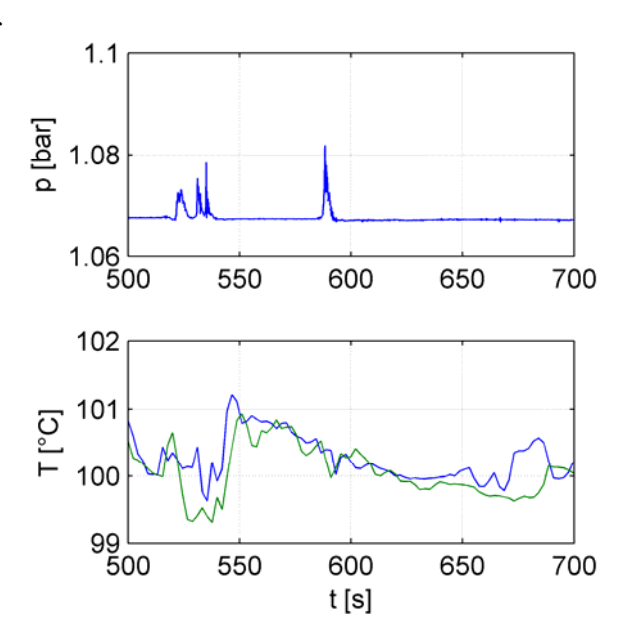


Fig. 2: Measured pressure peaks and temperature drop

3.2 Bubble visualisation

Observing the bubble behaviour delivers the most important information concerning modelling needs. As the front- and backside of the whole container is made of a single glass plate the visual accessibility is excellent. The growth-/shrink effect shown in Fig. 3 has been observed very often and is considered to be the most basic mechanism of propagation. The six images are consecutive with 0.1 seconds interval and for this image sequence the tracking was done manually. Inside the fluid volume spontaneous bubble growth can happen anywhere. The bubbles are then quickly pulled upwards by increased buoyancy. By encountering of a subcooled

layer the bubbles quickly condensate to sub-millimetre size. If the drag of the momentarily existent grown bubbles created enough upward motion in the liquid the effect may happen again and propagate into an eruption. If the encountered layering isn't subcooled at all the spontaneous bubble growth can also directly trigger an eruption.

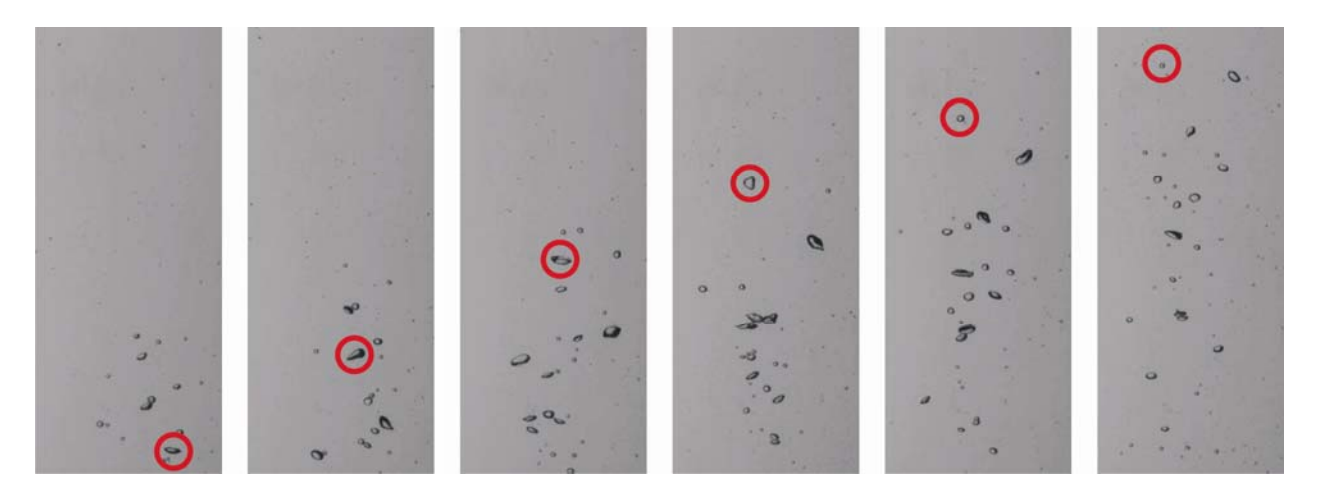


Fig. 3: Visualisation of the growth-/shrink effect

To analyse the video recordings several digital image processing steps are applied. The main operation is to separate the moving objects and the static background. Therefore, first the static background needs to be generated by arithmetically averaging each pixel of several images.

Frame differencing each frame from this static background separates the moving parts inside the picture. By increasing the contrast and following binarisation of the image it is possible to detect the so-called blobs as objects and gain several attributes. Essentially a blob is a local area of connected white or black pixels. To estimate its size the pixels are counted and by transformation into length coordinates the size is estimated. The perimeter is computed by calculating the distance between each adjoining pair of pixels around the border of the blob. The roundness can be determined by several methods, which are described in detail in [14]. As area and perimeter are available the following simple estimation for the roundness R = $p^2/(4\pi A)$ is calculated, where p is the perimeter and A is the projected area. The measurement of roundness has been checked applicability and it was established that

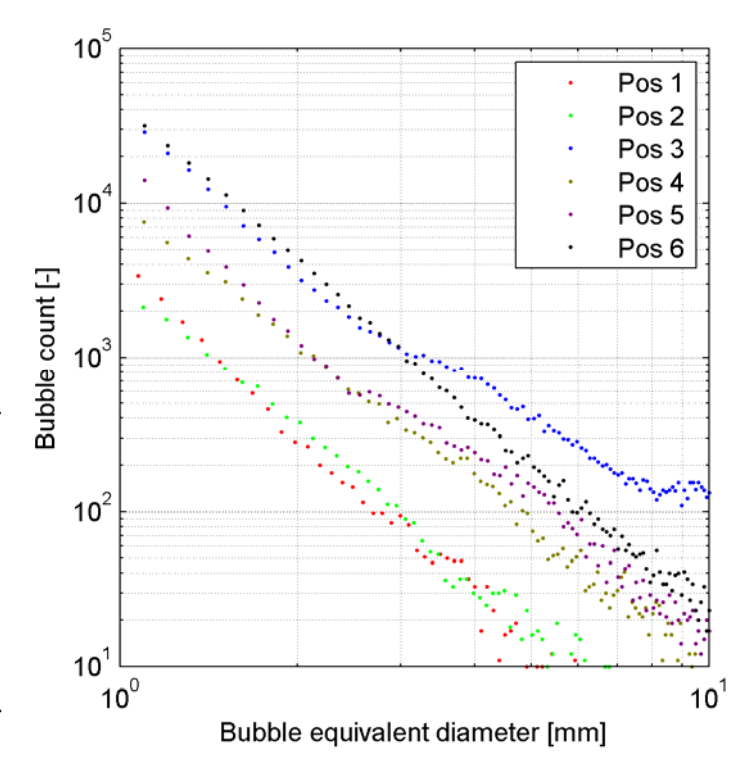


Fig. 4: Average bubble size distributions

bubble sizes up to 10 mm are sufficiently close to being circular. Hence it is assumed that if the projection is close to being circular the bubble can be considered as spherical.

The detected bubbles were sorted into size groups and the respective cumulated number of each size group is presented in Fig. 4. The average bubble size distribution shows the count of all detected bubbles (~6 million) within all measurement windows for a recording time of 140 minutes. The number of bubbles stays mostly constant with little standard deviation in the measurement interval of 1200 seconds. However, single peaks occur regularly (Fig. 5). Taking the average bubble size distribution into account and that the bubble number stays nearly constant it can be concluded that in this setup there is always a reservoir of nuclei, but not all of them become activated. Therefore, the number density of interest is the number of activated nuclei that grow to macroscopically sized bubbles. Since the experiment runs quasi-stationary the number of activated nuclei stays constant most of the time. Single events of instabilities cause a short increase in bubble number. Such instabilities cause a rapid temperature drop inside the volume that can be correlated to the level of present superheat. The sudden evaporation cools the liquid to saturation temperature.

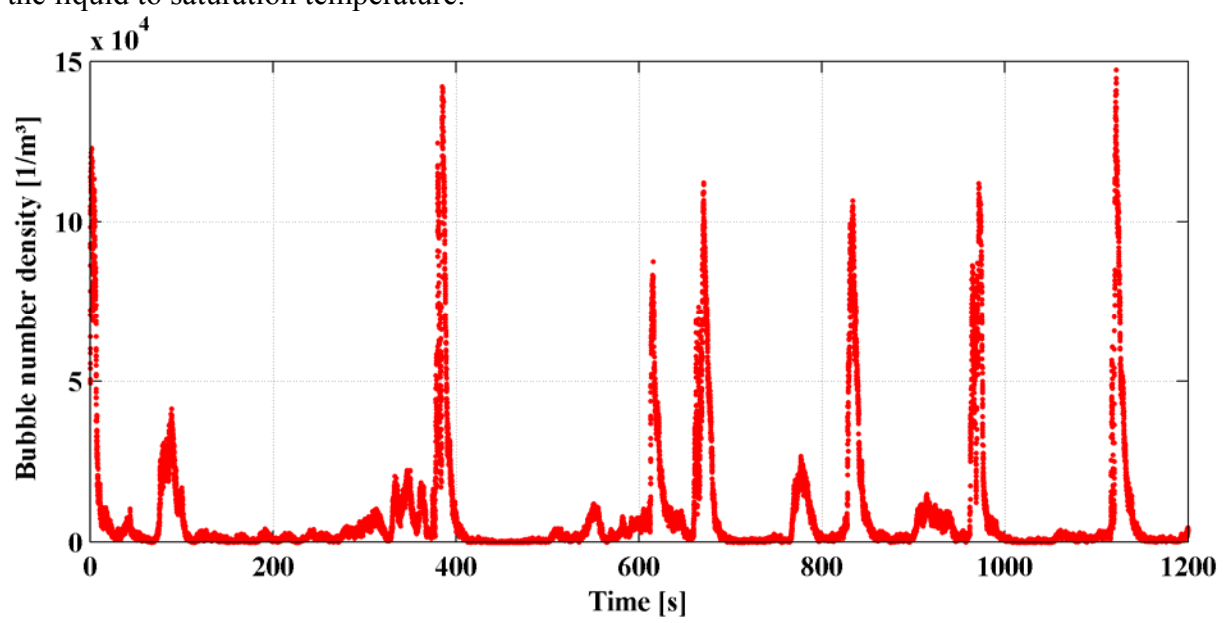


Fig. 5: Measured bubble number density

4. CFD-Modelling

4.1 General formulation

The commercial finite volume code CFX® is used as CFD software. It uses the Euler-Euler formulation introduced by Drew [11] which simulates an interpenetrating continuous and a dispersed fluid. The interactions between those two phases include several forces as well as energy and mass interchange. As previously discussed, one very central parameter is the bubble diameter which has to be prescribed for any simulation. Depending on the bubble diameter the evaporation is calculated as a simplified heat transfer problem following Péclets third order solution for stationary heat transfer. The simplifications consist of disregarding a temperature gradient inside the bubble volume (zero resistance) and an infinitesimal thin interfacial thickness as well as saturation temperature along the dividing surface. For calculation of the saturation

temperature T_{sat} the well-known Antoine equation is used with the pressure in Pa and the coefficients A = 8.0732991, B = 1656,390 and C = 226,86.

$$T_{sat} = \frac{B}{A \cdot \log_{10}(p/100)} - C \tag{4.1}$$

As problems with convergence arise upon definition of the saturation temperature depending on the pressure, it has been defined depending on the ordinate in the present simulations. Each bubble has a boundary layer surrounding the interfacial area and the heat transfer coefficient is calculated using the Ranz-Marshall correlation [12], where λ_I is the thermal heat conductivity of the liquid, d_b is the bubble diameter, Re and Pr are the Reynolds respectively Prandtl number.

$$h_b = \frac{\lambda_l}{d_b} \left(2 + 0.6 \,\text{Re}^{0.5} \,\text{Pr}_l^{0.33} \right) \tag{4.2}$$

As the Ranz-Marshall correlation depends on the Reynolds number the Bubble Reynolds number is modelled as [13] with the relative bubble velocity Δu , the bubble diameter d_b and the kinematic viscosity of the liquid v_1

$$Re = \frac{\Delta u \cdot d_b}{V_I}.$$
 (4.3)

The energy transfer instantaneously transfers mass by using the evaporation enthalpy at constant pressure. This way the vapour volume $\alpha \cdot V$ is calculated and usually the bubble diameter d_b is prescribed. This way the number of bubbles n is fixed.

$$\alpha \cdot V = n \cdot \frac{1}{6} \pi d_b^3. \tag{4.4}$$

4.2 CFD-Model

The proposed model for use in CFD calculation is applying a variable bubble number density depending on the local superheating conditions. The number density will be prescribed as a repository of micro bubbles, being a constant basic number density if the superheating or subcooling is low. This constant basic number of bubbles is as the measured average bubble number. As any driving heat difference causes evaporation and therefore cooling of the liquid, higher levels of superheating are only possible if the heat transfer is insufficient. The heat transfer coefficient and interfacial area limits the amount of heat that can be conveyed per time unit. As long as a bubble exists and the superheating is low no new bubbles are created, but the existing bubble grows. If the superheating rises and the heat exchange cannot provide equalisation it is necessary to increase the interfacial area by creation of new bubbles to counter superheating. Such superheating conditions correspond to the peaks previously shown in the experiments and can possibly cause instabilities. As these peaks strongly increase the bubble number, it is modelled using an exponential function. The algebraic function describing the bubble number density is therefore defined as

$$n = \begin{cases} A + e^{(B|T - T_{sat}|)} & \text{for } T - T_{sat} > 0 \\ A - e^{(B|T - T_{sat}|)} & \text{for } T - T_{sat} < 0 \end{cases}$$
(4.5)

The model parameter A corresponds to the average bubble number density and the parameter B corresponds to the level of superheating that causes a sharp increase in the bubble number density. The level of superheating is estimated by the local temperature drop measured during

the flashing events as the temperature should drop to saturation temperature. The parameters used in the calculations are estimated with the values A = 20000 and B = 1. Using the local number density the bubble diameter is calculated and prescribed to the calculation with values ranging from 0.1 mm up to 10 mm.

5. CFD-Calculations

The CFD calculations were performed with Ansys CFX® 12. The water column has been reduced to 380x380x10 mm and the depth is reduced for a quasi-2D simulation (two cells). The mesh is very coarse with 3042 Elements, and a mesh sensitivity study is yet to be performed. The top face of the volume is configured as opening boundary with the opening temperature being at saturation temperature. The front and back area are modelled using translational periodicity. All remaining faces are adiabatic walls with no slip condition. As a transient calculation with a duration of 5 s is performed, the pressure is initialised hydrostatically, the velocities are all set to zero and the initial vapour volume fraction is $1x10^{-6}$. The temperature is initialised in three different ways: The temperature distribution is 2 K/1 K/0 K below saturation temperature and a single hotspot with 1 K above saturation temperature exists centered in the volume (Fig. 6).

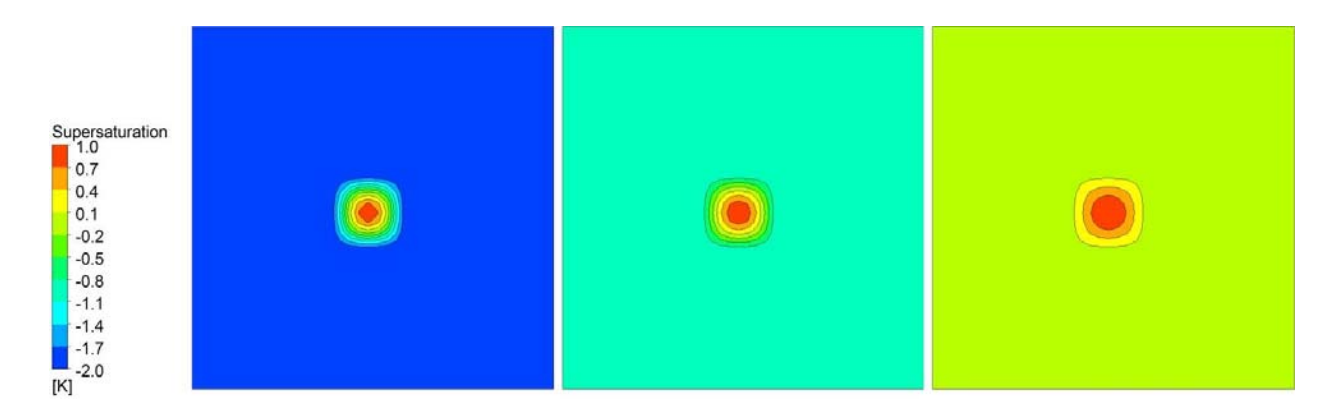


Fig. 6: Initialisation of the subcooling: 2K (left), 1K (center) and 0K (right)

As this hotspot starts to cause evaporation the bubbles rise and drag the hotspot upwards additionally to the natural convection. This shortens the duration of the transient and reduces computational cost as the time steps are in a range of 1×10^{-4} s. These initialisations represent the described growth/-shrink effect that can propagate into an instability depending on the layering and therefore the release of energy available to evaporation. The calculation shows that the implemented model can reproduce locally changing bubble sizes i.e. the growth/-shrink effect that takes place under variation of the vapour fraction (Fig. 7). It can be seen that the movement of the liquid hotspot is dependent on the vapour creation, as with higher subcooling the hotspot passes the monitor point at a later time. The higher subcooling quickly causes recondensation of the bubbles in the layer above the hotspot and therefore suppresses the hotspots movement. In Fig. 7 a monitor point above the hotspot is used to monitor the passing hotspot and observe the bubble size progression. At high subcooling the bubble number density is exponentially decreased as seen in (4.5). Thus, the remaining vapour is distributed towards a single bubble per m³ and this results in a large local bubble size. This effect doesn't seem physical and is under

investigation. As higher values of supersaturation increase the interfacial area by increasing the bubble number density the average bubble size decreases. This corresponds to the previously shown bubble size distribution as with lower size there are more bubbles, and therefore the average size drops.

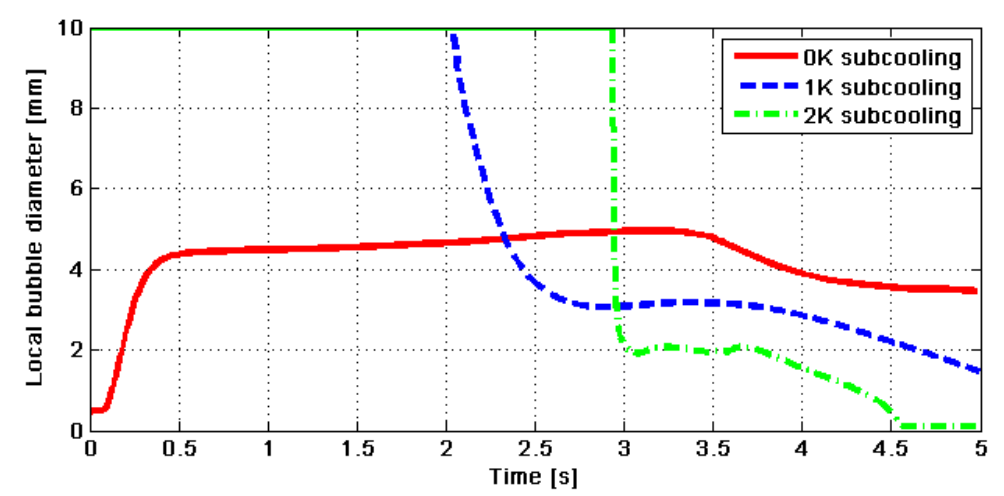


Fig. 7: Progression of the bubble diameter

6. Conclusion

An experimental setup with several temperature and pressure measurement sensors has been built. It offers large glass areas for bubble observation that enables video recordings which can be evaluated digitally. Thus, additional data about bubbles such as bubble numbers as well as additional properties are available. The bubble size distribution always resolve to an exponential behaviour, indicating that there is a pool of small bubbles available for mass transfer and further growth. In case of sudden evaporation consequently a rise in bubble number causes a decrease in average bubble size. Upon a flashing event the temperature inside the container drops towards saturation temperature. It has been experimentally shown that the bubble number and the mean size show no direct correlation to each another and they aren't necessarily associated with an instability. Sudden evaporation often occurs but due to the growth-/shrink in consequence of the local thermal layering these bubbles can as suddenly re-condensate. If a hotter layering is encountered the bubbles can keep growing and induce a quickly rising plume of hot water that propagates towards lower pressure and therefore lower saturation. This causes latent heat to become available and therefore becomes an instability.

A CFD model has been proposed that accounts for the discussed main effects. It has been implemented into CFX® and calculations were conducted to re-produce the mechanisms described above. The growth-/shrink mechanism is successfully reproduced using the algebraic formulation. It has been shown that the subcooling of the surrounding liquid is responsible for the bubble propagation which influences the upward transport of hot water portions. Without enough drag from the grown bubbles the hotspot cannot propagate into lower pressure regions were it could release latent heat for evaporation. The model needs to be tested further to prove the quantitative quality of the prediction.

Acknowledgement

This work is carried out in the frame of a current research project (project number 1501364) funded by the German Federal Ministry of Economics and Technology.

7. References

- [1] M. Volmer, A.Weber. "Keimbildung in übersättigten Gebilden", Zeitschrift f. phys. Chemie 119, S. 277-301, 1926
- [2] R. Becker, W. Döring, "Kinetische Behandlung der Keimbildung in übersättigten Dämpfen", Ann. Phys. 24, 719, Leipzig, 1935
- [3] R. C. Miller, R. J. Anderson, J. L. Kassner, Jr., and D. E. Hagen. "Homogeneous Nucleation Rate Measurements for Water over a Wide Range of Temperature and Nucleation Rate." Journal of Chemical Physics 78, no. 6 (1983): 3204–3211.
- [4] Y. Viisanen, R. Strey, and H. Reiss. "Homogeneous Nucleation Rates for Water." Journal of Chemical Physics 99, no. 6 (1993): 4680–4692.
- [5] J.Wölk, R. Strey, C. H. Heath, and B. E. Wyslouzil. "Empirical function for homogeneous water nucleation rates." Journal of Chemical Physics 117, no. 10 (2002): 4954–4960.
- [6] S. Rong, Y. Mi, M. Ishii, and M. Mori. "Photographic study of bubble behaviours forced convection subcooled boiling." International Journal of Heat and Mass Transfer 47 (2004): 3659–3667.
- [7] A. Zaruba, E. Krepper, H. M. Prasser, and B. N. Reddy Vanga. "Experimental Study on Bubble Motion in a Rectangular Bubble Column using High-Speed Video Observations." Flow Measurement and Instrumentation 16 (2005): 277–287.
- [8] M. Daubner, G. Janssens-Maenhout, J.U. Knebel. "Technische Beschreibung der Testanlage SUCOT zur Untersuchung einer Wasser / Wasserdampf Zweiphasenströmung", Report FZKA 6683, Forschungszentrum Karlsruhe GmbH, Karlsruhe, 2002.
- [9] T. Giese, "Numerische und experimentelle Untersuchung von gravitationsgetriebenen Zweiphasenströmungen durch Rohrleitungen", Dissertation, Stuttgart: University, 2003
- [10] E. Laurien, "Influence of the model bubble diameter on three-dimensional numerical simulations of thermal cavitation in pipe elbows", 3rd International Symposium on Two-Phase Flow Modelling and Experimentation, Pisa, 22-24 September 2004
- [11] D.A. Drew, "Mathematical Modelling of Two-Phase Flows", Ann. Rev. Fluid Mech. 15, pp. 261-291, 1998
- [12] W.E. Ranz, W.R. Marshall. "Evaporation from Drops", Chemical Engineering Progress 48, 1952, Part I: 141-146, Part II: 173-180
- [13] R. Clift, J.R. Grace and M.E. Weber. "Bubbles, Drops and Particles", Academic Press, New York, San Francisco, London, 1978

[14] J. Kutnjak, R. Kulenovic, E. Laurien. "Experimental Investigation of Vapour Bubbles Nucleating in Bulk Liquid", HEFAT 2010, 7th International Conference on Heat Transfer, Fluid Mechanics and Thermodynamics, 19.-21. July 2010, Antalya, Turkey